IOP Conf. Series: Journal of Physics: Conf. Series **844** (2017) 012050 doi:10.1088/1742-6596/844/1/012050

Algorithm for Evaluation of Temperature 3D-Distribution of a Vapor Cell in a Diode End-pumped Alkali Laser System

J H Han, Y Wang*, H Cai, G F An, K P Rong, H Yu, S Y Wang, H Y Wang, W Zhang, L P Xue and J Zhou

Southwest Institute of Technical Physics, Chengdu, Sichuan 610041, China

*Corresponding Author. E-Mail: youwang_2007@aliyun.com

Abstract. We develop a new 3D-model to evaluate the light characteristics and the thermal features of a cesium-vapor laser end-pumped by a laser diode. The theoretical model is based on the principles of both heat transfer and laser kinetics. The 3-dimensional population density distribution and temperature distribution are both systematically obtained and analyzed. The methodology is thought to be useful for realization of a high-powered diode-pumped alkali laser (DPAL) in the future.

1. Introduction

With narrow linewidth, high Stokes-efficiency, compact size, good thermal performance, non-toxic system, etc., a diode-pumped alkali laser (DPAL) becomes one of the most hopeful high-powered laser sources of the next generation and has been rapidly developed since the beginning of the 21th century [1-5]. However, the thermal effects will bring about some serious problems in nonuniformity of the temperature distribution for a high-powered DPAL system because the thermal conductivity of a gas-state medium is so small that the generated heat cannot be transferred outside efficiently [6-9]. Unlike a conventional electrically-excited gas-state laser, the number densities of alkali vapors (gain gas) and buffer gases (generally being helium and small hydrocarbons such as methane and ethane) in a DPAL often exhibit inhomogeneous distributions resulting from the temperature gradient inside a vapor cell [10, 11]. Actually, the inhomogeneous of the alkali vapor directly influences the output performances of a DPAL. Furthermore, the nonuniformity of buffer gases affects the line-center collisionally broadened cross sections of both the D_1 line ($n^2P_{1/2} \rightarrow n^2S_{1/2}$) and the D_2 line ($n^2S_{1/2} \rightarrow n^2P_{3/2}$) of an alkali atom as well as the finestructure mixing rate ($n^2P_{3/2} \rightarrow n^2P_{1/2}$) [12-15].

2. Experimental Setup

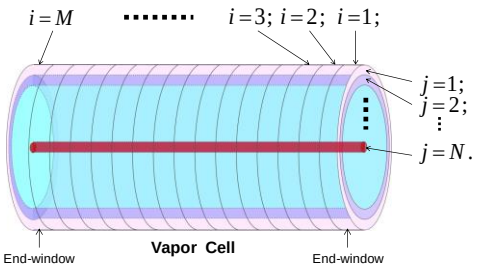

Figure 1. Schematic illustration for segmentation of a gain media cell.

For an end-pumped DPAL configuration, the optical axis of a pump laser diode coincides with that of the output laser. As shown in Figure 1, we divide the cylindrical gas vapor cell into many cylindrical annuli along the optical axis direction with i = 1, 2, 3…M and the transversal surface direction with j = 1, 2, 3 …N. Every small cylindrical annulus is thought as a heat source and a gain source. Both the gain and the heat generated in the cylindrical annulus are different with each other.

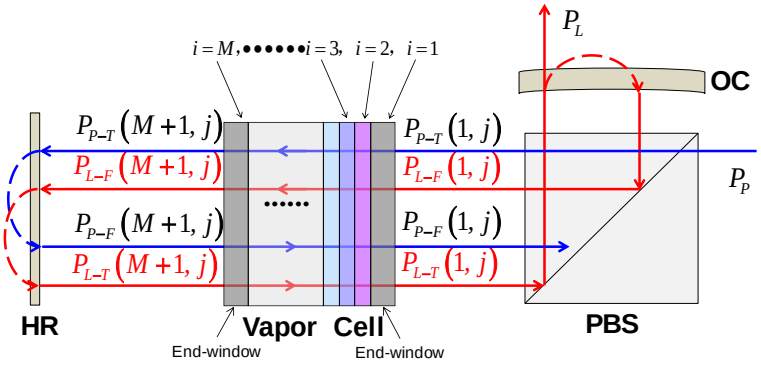

Figure 2. Schematic illustration showing pump and laser propagation directions at various points as the pump and laser fluence traverses the gain media in a double-pass geometry.

The pump and laser energies at the outside surface of the end-windows as the pump and laser fluence goes through the gain medium in double-pass geometry can be expressed by

$$\begin{cases} P_{P-T}(1,\ j) = \eta_{del} P_P^j \\ P_{P-F}(M+1,\ j) = R_{\mathrm{HR}} \cdot P_{P-T}(M+1,\ j) \end{cases}, \tag{1}$$

and

$$\begin{cases} P_{L-F}(1,\ j) = R_{\mathrm{OC}} \cdot P_{L-T}(1,\ j) \\ P_{L-T}(M+1,\ j) = R_{\mathrm{HR}} \cdot P_{L-F}(M+1,\ j) \\ P_L^j = (1-R_{\mathrm{OC}}) \cdot P_{L-T}(1,\ j) \end{cases}. \tag{2}$$

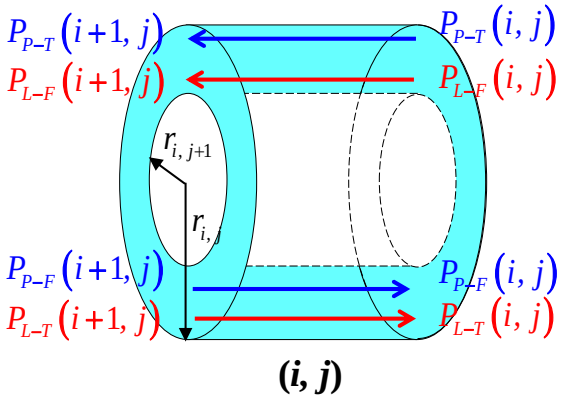

Figure 3. Diagram describing the power changes when the pump and laser fluence traverses the (i, j) cylindrical annulus.

As shown in Figure 3, we select an arbitrarily cylindrical annulus (i, j) among the segments to analyze the laser and heat features. $P_{P\text{-}T}$ (i, j) and $P_{P\text{-}F}$ (i, j) are the pump power corresponding to the (i, j) cylindrical annulus transferred towards the left and right (reflected back from the high reflector),

respectively. $P_{L\text{-}F}(i, j)$ and $P_{L\text{-}T}(i, j)$ are the laser power corresponding to the (i, j) cylindrical annulus transferring towards the left (reflected back from the output coupler), respectively.

The relationships between $P_{P\text{-}T}(i, j)$ and $P_{P\text{-}T}(i+1, j)$, $P_{P\text{-}F}(i, j)$ and $P_{P\text{-}F}(i+1, j)$, $P_{L\text{-}T}(i, j)$ and $P_{L\text{-}T}(i+1, j)$, $P_{L\text{-}F}(i, j)$ and $P_{L\text{-}F}(i+1, j)$, can be respectively given by

$$\begin{cases} P_{P-T}(\mathrm{i},j)\exp\left[-\left(n_1^j-\frac{1}{2}n_3^j\right)\sigma_{D_2}(T_j,\lambda)\frac{\mathrm{L}}{\mathrm{M}}\right]=P_{P-T}(\mathrm{i}+1,j) \\ P_{P-F}(\mathrm{i}+1,j)\exp\left[-\left(n_1^j-\frac{1}{2}n_3^j\right)\sigma_{D_2}(T_j,\lambda)\frac{\mathrm{L}}{\mathrm{M}}\right]=P_{P-F}(\mathrm{i},j) \end{cases}, \tag{3}$$

and

$$\begin{cases} P_{L-T}(i+1,j)\exp\left[\left(n_2^{(i,j)}-n_1^{(ij)}\right)\sigma_{D_1}^{He-broadened}(i,j)\frac{\mathrm{L}}{\mathrm{M}}\right]TT^{1/N}=P_{L-T}(i,j) \\ P_{L-F}(i,j)\exp\left[\left(n_2^{(i,j)}-n_1^{(i,j)}\right)\sigma_{D_1}^{He-broadened}(i,j)\frac{\mathrm{L}}{\mathrm{M}}\right]TT^{1/N}=P_{L-F}(i+1,j) \end{cases}. \tag{4}$$

The equated power of the pump and the laser power can be simply expressed by

$$P_P(i,j)=P_{P-T}(i,j)+P_{P-F}(i+1,j), \tag{5}$$

and

$$P_L(i,j)=P_{L-T}(i,j)+P_{L-F}(i+1,j). \tag{6}$$

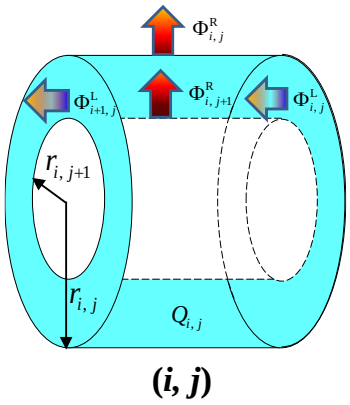

Figure 4. Drawing of illustrating heat generated and transferred for the (i, j) cylindrical annulus of a vapor cell.

Next, the heat characteristics can be shown as Figure 4. The relationship between the *input heat* and the *output heat* as well as the *generated heat* the can be described as

$$\Phi^{R}_{i,j}+Q_{i,j}+\Phi^{R}_{i,j+1}=\Phi^{L}_{i+1,j}+\Phi^{L}_{i,j}. \tag{7}$$

Then, we calculate the population distribution in a three energy-level system of the (i, j) cylindrical annulus (see Figure 3) by using the well-known rate equations as follows [5, 11, 12]:

$$\begin{cases} \frac{dn_1(i,j)}{dt}=-\Gamma_P(i,j)+\Gamma_L(i,j)+\frac{n_2(i,j)}{\tau_{D_1}}+\frac{n_3(i,j)}{\tau_{D_2}} \\ \frac{dn_2(i,j)}{dt}=-\Gamma_L(i,j)+\gamma_{32}(T_{i,j})\left[n_3(i,j)-2n_2(i,j)\exp\left(-\frac{\Delta E}{k_BT_{i,j}}\right)\right]-\frac{n_2(i,j)}{\tau_{D_1}} \\ \frac{dn_3(i,j)}{dt}=\Gamma_P(i,j)-\gamma_{32}(T_{i,j})\left[n_3(i,j)-2n_2(i,j)\exp\left(-\frac{\Delta E}{k_BT_{i,j}}\right)\right]-\frac{n_3(i,j)}{\tau_{D_2}} \end{cases}. \tag{8}$$

We calculate the volume density of generated heat of the (*i, j*) cylindrical annulus by using the following formula:

$$Q_{i,j} = V_{i,j} \cdot \gamma_{^2P_{3/2}\to{}^2P_{1/2}}\left(T_{i,j}\right)\left[n_3(i,j) - 2n_2(i,j)\exp(-\frac{\Delta E}{k_B T_{i,j}})\right]\Delta E \quad . \tag{9}$$

By utilizing the theoretical model, the thermal features and the physical characteristics of a DPAL can be obtained.

3. Results and Discussions

By using the theoretical model introduced in Section 2, we calculate the physical characteristics of a DPAL and the thermal features of a cesium cell. The relevant parameters are listed in Table 1.

Table 1. Parameters for evaluating temperature distribution of a Cs vapor cell

Parameter Description	Values
Partial pressure of He	500 Torr
Partial pressure of C_2H_6	100 Torr
η_{del}	90%
L	25 *mm*
R	5 *mm*
T_W	100 ℃
Pump power	100 W
End-windows thickness	1 *mm*
R_{OC}	30%
Room temperature	20 ℃
Pump FWHM	30 GHz
Center wavelength of the pump	852.3 *nm*
D_1 transition wavelength	894.6 *nm*
Laser beam waists	0.5 *mm*
Pump beam waists	1.1 *mm*

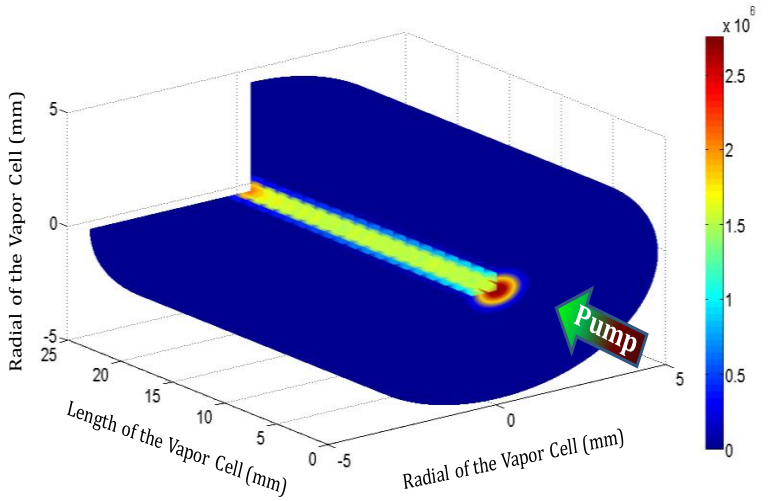

Figure 5. 3-D distribution of absorbed pump density inside a cesium cell.

We first analyze the distribution of absorbed pump density inside a vapor cell. As shown in Figure 5, the absorption of gas medium nearby the two end-windows is much stronger than those around the central area. The reason is that the pump power is high enough to make the gas medium around the central core be absorbed adequately, and the gas medium density nearby the end-windows is higher than that around the central core since the temperatures nearby the end-windows are lower than those in the other places. The laser density of the pump input side is higher than another side (see Figure 6) as the gain of the input side is higher than another one.

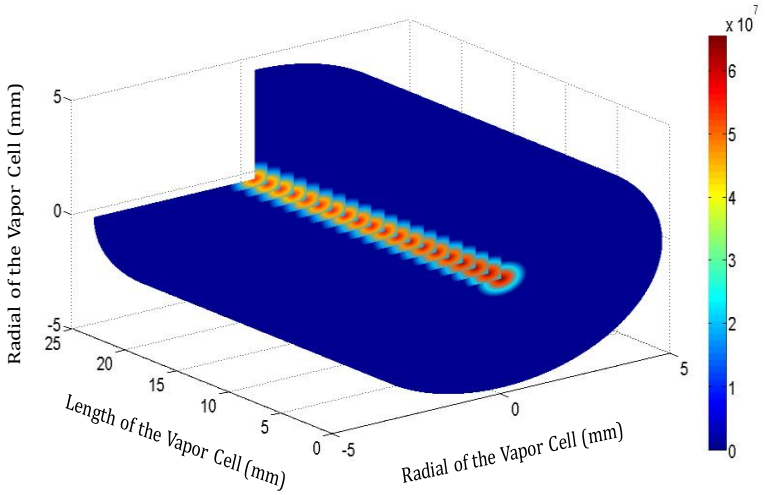

Figure 6. 3-D density distribution of laser intensity inside a cesium cell.

As shown in Figure 7, the temperature distribution exhibits a distinct gradient and achieves the maximum values at the central axis of the cell. Such tendencies can be explained by a fact that the thermal conductivity of a gas-state medium is so small that the generated heat cannot be transferred outside efficiently. It can be found that the absorbed pump power leads to a more obvious temperature rise for a static medium. The maximum temperature rise even reaches about 550 K at the cell axis. However, such a temperature gradient can be effectively decreased with a flowing approach. The published literatures have proven that the flowing-gas procedure is essential and effective to construct an even-higher DPAL system.

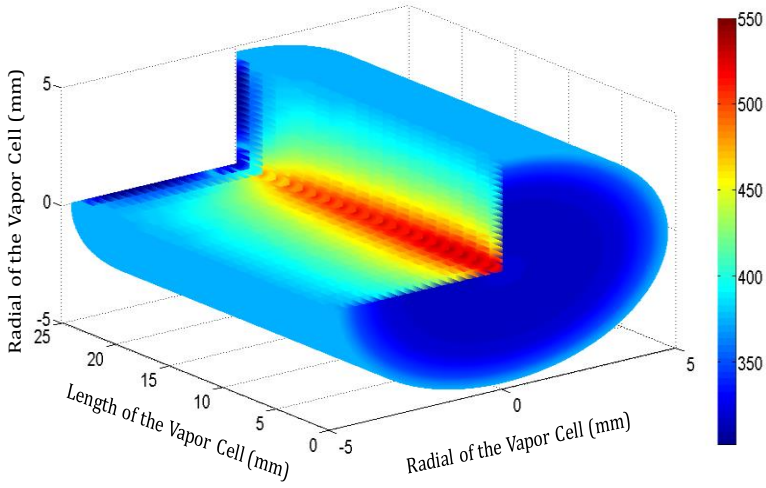

Figure 7. 3-D temperature distribution of a cesium cell.

4. Conclusions

In this report, we present the results of theoretical studies on the thermal features of a cesium vapor cell pumped by a laser diode. A theoretical model is developed by combining the procedures of laser kinetics and heat transfer together.

The temperature around the cell axis is somewhat higher than the other positions inside the cell. The highest temperature is located at the central optical axis near the pump input side. The absorption efficiency, gain intensity and generated thermal power near the pump input side are much stronger than those near the opposite side.

References

[1] Krupke W F, Beach R J, Kanz V K and Payne S A 2003 *Opt. Lett.* **28** 2336–2338
[2] Page R H, Beach R J, and Kanz V K5 2006 *Opt. Lett.* **31** 353–355
[3] Zhdanov B V and Knize R J 2007 *Opt. Lett.* **32** 2167–2169
[4] Wang Y, Niigaki M, Fukuoka H, Zheng Y, Miyajima H, Matsuoka S, Kubomura H, Hiruma T, and Kan H 2007 *Phys. Lett. A* **360** 659–663
[5] Cai H, Wang Y, Xue L P, Zhang W, Han J H, Wang H Y, and An G F 2014 *Appl. Phys.* B **117** 1201–1210
[6] Zhu Q, Pan B L, Chen L, Wang Y J, and Zhang X Y 2010 *Opt. Commun.* **283** 2406–2410
[7] Barmashenko B D and Rosenwaks S, 2013 *Opt. Soc.* Am. B **30** 1118–1126
[8] Barmashenko B D and Rosenwaks S 2013 *Appl. Phys. Lett.* **102** 141108–141111
[9] Rosenwaks S, Barmashenko B D, and Waichman K 2014 *Proc. SPIE **8962*** 311–316
[10] Steck D A 2010 Available online at http://steckus/alkalidata
[11] Han J H, Wang Y, Cai H, Zhang W, Xue L P, and Wang H Y 2014 *Opt. Express.* **22** 13988–14003
[12] Beach R J, Krupke W F, Kanz V K, and Payne S A 2004 *J. Opt. Soc. Am. B* **21** 2151–2163
[13] Yang Z, Wang H, Lu Q, Hua W, and Xu X 2011 *Optics. Express* **19** 23118
[14] Bogachev A V, Garanin S G, Dudov A M, Yeroshenko V A, Kulikov S M, Mikaelian G T, Panarin V A, Pautov V O, Rus A V, and Sukharev S A 2012 *Quantum Electronics* **42** 95–98
[15] Rice C A, Lott G E, and Perram G P 2012 *Appl. Opt.* **51** 8102–8110